GEOLOGICA CARPATHICA, 2024, 75, 2, 117–131 https://doi.org/10.31577/GeolCarp.2024.06

Mineralogy and genesis of sapphire in corundum-bearing xenoliths from the Miocene andesites in the Záhradné, Hubošovce and Vechec quarries in the Slanské vrchy Mountains (Slovakia)

PAVOL MYŠĽAN[1,2,✉], MARTIN ŠTEVKO[1,3], TOMÁŠ MIKUŠ[4] and TOMÁŠ VACULOVIČ[5,6]

[1]Earth Science Institute, Slovak Academy of Sciences, Dúbravská cesta 9, P. O. BOX 106, 840 05 Bratislava, Slovakia
[2]Department of Mineralogy, Petrology and Economic Geology, Faculty of Natural Sciences, Comenius University in Bratislava, Ilkovičova 6, Mlynská dolina, 842 15 Bratislava, Slovakia
[3]Department of Mineralogy and Petrology, National Museum, Cirkusová 1740, 193 00 Praha 9 – Horní Počernice, Czech Republic
[4]Earth Science Institute, Slovak Academy of Sciences, Ďumbierska 1, 974 11 Banská Bystrica, Slovakia
[5]Department of Chemistry, Faculty of Science, Masaryk University, Kamenice 5, 625 00, Brno, Czech Republic
[6]Institute of Laboratory Research on Geomaterials, Faculty of Natural Sciences, Comenius University in Bratislava, Ilkovičova 6, Mlynská dolina, 842 15 Bratislava, Slovakia

(Manuscript received March 4, 2024; accepted in revised form May 20, 2024; Associate Editor: Peter Bačík)

Abstract: Sapphires crystals were identified in the corundum-bearing xenoliths in Miocene (Upper to Middle Sarmathian) andesites of the Slanské vrchy Mountains, eastern Slovakia at the Záhradné, Hubošovce and Vechec localities. The sapphire crystals occur in (1) micaceous xenoliths, which are built mostly of dark mica from annite–phlogopite series (biotite), K-feldspars, plagioclase with abundant inclusions of hercynite, ilmenite and Ti-rich magnetite, locally with pyroxenes of enstatite-ferosilite series at the localities Záhradné and Hubošovce. Less abundant are sapphires occurring in cordieritic xenoliths (2), dominantly consisting of cordierite, plagioclase and sillimanite with minor hercynite and ilmenite inclusions discovered in the Vechec quarry. Sapphires are dark blue to light blue with vitreous to diamond lustre and no visible pleochroic colour change forming mostly pseudohexagonal tabular, locally more complex euhedral to subhedral crystals up to 2.0 mm in size with triangular-shaped patterns on crystal faces. Raman spectroscopy showed characteristic corundum peaks at 419 cm^{-1} A_{1g} mode and 384 cm^{-1} E_g mode with other peaks assigned to Al_2O_3 crystal vibrations. Chemical composition (EPMA, LA-ICP-MS) shows typical content of 98.12–99.60 wt. % Al_2O_3 with increased concentrations of Fe, Ti, Cr, V, Mg and Ga, locally also Na, Ca, K, B and Li. Genesis of corundum-bearing xenoliths interpreted from paragenetic observations and geochemical data shows clear metamorphic trend. Formation of sapphires was caused by incorporation of Al-rich precursor metasediments depleted in silica into the magmatic reservoir, which caused thermal overprint of the precursor mineral assemblage and led to the formation of high temperature mineral association suitable for corundum crystallization. Furthermore, sapphire crystals from the Hubošovce quarry exhibit spinel coronas, which are typically developed from destabilization of corundum during their retrograde development.

Keywords: Slanské vrchy Mts., Záhradné, Hubošovce, Vechec, xenolith, corundum, sapphire

Introduction

Sapphire is known as a blue variety of corundum, which has a trigonal crystal structure belonging to the $R\bar{3}c$ space group. The crystal structure of corundum consists of O atoms arranged in hexagonal close packing with Al atoms occupying two thirds of the octahedral sites (Ishizawa et al. 1980). Corundum is a very well-known mineral from the different environments in Al-rich and Si-poor igneous, metamorphic (anatectic, metasomatic), weathering and alluvial sedimentary deposits (e.g., Giuliani et al. 2005, 2014, 2020; Simonet et al. 2008; Sorokina et al. 2017; Miranda-Díaz et al. 2022) all around the world.

Aluminium oxide occurs in the form of several allotropic modifications, where corundum exists in the form of α-Al_2O_3, other modifications are known as synthetic equivalents, or they rarely occur in nature. Natural δ- and θ-Al_2O_3 were reported from permafrost sediments in Russia (Zigert et al. 1990), χ-Al_2O_3 was found in lateritic pisolites in Australia (Singh & Gilkes 1995) or η-Al_2O_3 was identified in bauxites from Queensland, Australia (Tilley & Eggleton 1996). Recently, only deltalumite, the tetragonal δ-Al_2O_3 modification with the spinel structure, was described as a valid mineral from the pores of basalt lava and scoria altered by fumarolic gas at Ploskiy Tolbachik Volcano in Russia with a structural formula written as $(Al_{0.67}\square_{0.33})Al_2O_4$ (Pekov et al. 2019).

✉ corresponding author: Pavol Myšľan
pavol.myslan@savba.sk

In the Neogene volcanic area in the Western Carpathians of Slovakia and Hungary, corundum (α-Al_2O_3) is a rare accessory mineral. Occurrences of sapphire are documented from the andesites, pyroclastic rocks and hornfels of the Štiavnické and Kremnické vrchy Mts. at the localities Sklené Teplice and Dolné Hámre (Hvožďara & Činčár 1972), Dobrá Niva (Fiala 1954) and borehole KR-3 near Kremnica (Böhmer & Šímová 1976), in the xenoliths detected in boreholes KŠ-8 and KŠ-33 near Klokoč and Stožok in the Javorie Mts. (Kollárová & Hraško 2009), in the xenoliths in andesites from Vechec in the Slanské vrchy Mts. (Ďuďa et al. 1981) and in the Börzsöny and Visegrád Mts. (Szakáll et al. 2002). Sapphire also occurs in primary volcanic Neogene Al–Si metasomatic bodies at the locality Remetské Hámre – Kapka in the Vihorlatské vrchy Mts. (Bacsó 1971; Derco et al. 1977) and Vígľašská Huta in the Javorie Mts. (Marková & Štohl 1978). Furthermore, sapphire occurs in Pliocene–Pleistocene alkali basalts at the localities Hajnáčka and Gortva (Uher et al. 2012), in syenitic xenoliths in the Pliocene maar at Pinciná in the Cerová Highlands (Hurai et al. 1998; Huraiová & Konečný 2006) and as amoeboid corundum exsolutions from plagioclase in xenoliths in Čamovce basalt quarry (Reato et al. 2022).

Aim of this work is focused on the detailed mineralogical characterization of the main and accessory minerals of the corundum-bearing xenoliths from the three studied localities in the Slanské vrchy Mts. as well as detailed spectrometric (Raman) and chemical (EPMA-WDS, LA-ICP-MS) study of the corundum crystals. These parameters are also discussed on behalf of the probable corundum origin.

Geological settings and localization

The Slanské vrchy Mts. belong to the Eastern Slovakian Neovolcanic mountain chain (Fig. 1a) generated during the Miocene volcanic activity. The oldest geological superunit present in the bedrock of the northern part of Slanské vrchy Mts. is Veporicum with lithological sequences composed of Paleozoic crystalline rocks (migmatites, granodiorites and amphibolites) of the Čierna hora Belt (Fig. 2b). The Permian units of the Ľubietová Group are deposited on the underlying crystalline units and consist mostly of arkoses and cherts. Paleozoic units are overlain by Mesozoic (Lower Triassic to Lower Jurassic) sedimentary rocks of continental and shallow-water origin. Peripherally, the underlying sequences of the Eastern part of the Slanské vrchy Mts. belong to the Iňačovce–Kričevo Unit, built mostly by metamorphosed ultramafic rocks, basalts, tuffites and pelitic rocks (Kaličiak et al. 1991; Vass et al. 2000).

The studied area in the northern part of the Slanské vrchy Mts. is built by Lysá Stráž–Oblík in the form of extrusive andesites and shallow intrusive diorite porphyries, which are situated in the NW–SE volcanic-tectonic zone (Kaličiak et al. 1991). Studied xenoliths occur in the Maliniak and Lysá Stráž igneous bodies, which are part of the Lysá Stráž–Oblík Formation (Fig. 1c). The magmatic activity of the extrusive bodies is dated based on FT method in the interval 12.2 ±0.4 Ma, which corresponds to the Upper Sarmatian period (Kaličiak & Repčok 1987). The magma of the studied formation was probably formed at mantle–crust boundary and crystallized in temperature–pressure conditions determined in the temperature interval of 810–940 °C and above 800 MPa for Maliniak andesite body and 900–1000 °C at a pressure about 600–700 MPa for Lysá Stráž body (Bónová 2005).

Extrusive domes and bodies are composed of a light gray pyroxenic–amphibole andesites with minor garnet. The most common rock-forming minerals are plagioclase ($An_{61–77}$), Ca-amphibole, enstatite–ferosilite and augite with accessory garnet grains of dominantly almandine composition. Apatite, zircon, ilmenite and magnetite are present in the form of accessory minerals. Minerals are partially carbonatized and chloritized (Zorkovský 1953; Bónová 2005). The bodies of the Lysá Stráž–Oblík Formation are overlaid with volcanic products of the Zlatá Baňa Formation (Upper Sarmatian–Lower Pannonian) and occur in the environment of sedimentary rocks of the Subtatric Group of the Inner Carpathian Paleogene. Andesites cut through Paleogene clay shales and sandstones of the Zuberec Formation (Kaličiak et al. 1991), which are partially metamorphosed at the contact with andesite.

Most of xenoliths in the Záhradné quarry are formed by volcano-sedimentary and pelitic sedimentary rocks and porcelanites. The genesis of these xenoliths was addressed by Marcinčáková & Košuth (2011), who assume that the xenoliths containing clastic rock fragments from the Záhradné originated from Neogene to Paleogene sedimentary protolith. Moreover, basic magmatic enclaves were identified in the Hubošovce quarry, which are composed of pyroxene, plagioclase and rarely garnet and biotite, locally accumulated at the contact with andesite (Marcinčáková & Košuth 2011).

The second area studied in this work occurs in the middle part of the Slanské vrchy Mts. Volcanic formation is composed of the remains of the parasitic Vechec andesite stratovolcano situated between the Makovica and Strechový vrch stratovolcanoes (Fig. 1c). The central zone of the Vechec stratovolcano is formed by a volcanic neck. The volcanic cone and mantle, which are located on the outer zone of the volcano, are formed by the relics of lava flows, composed of predominantly grey to grey-black pyroxene andesite. The effusive andesite products of the parasitic Vechec stratovolcano are formed mostly by plagioclase ($An_{40–50}$) and pyroxenes, mainly augite and enstatite–ferrosilite series. The peripheral zone consists mainly of redeposited andesite pyroclastic material and tuffs (Kaličiak et al. 1991). Radiometric dating using the K–Ar method estimated the age of the andesite in the central part of the stratovolcano at 11.8 Ma (Ďurica et al. 1978), which classifies the formation of stratovolcano to Central Sarmatian volcanic activity.

Both the Záhradné and the Hubošovce quarries ale located approximately 10 km NE of Prešov town. The Záhradné quarry is situated in the root part of the Maliniak extrusive dome, located 2 km SW of the same name village, its GPS

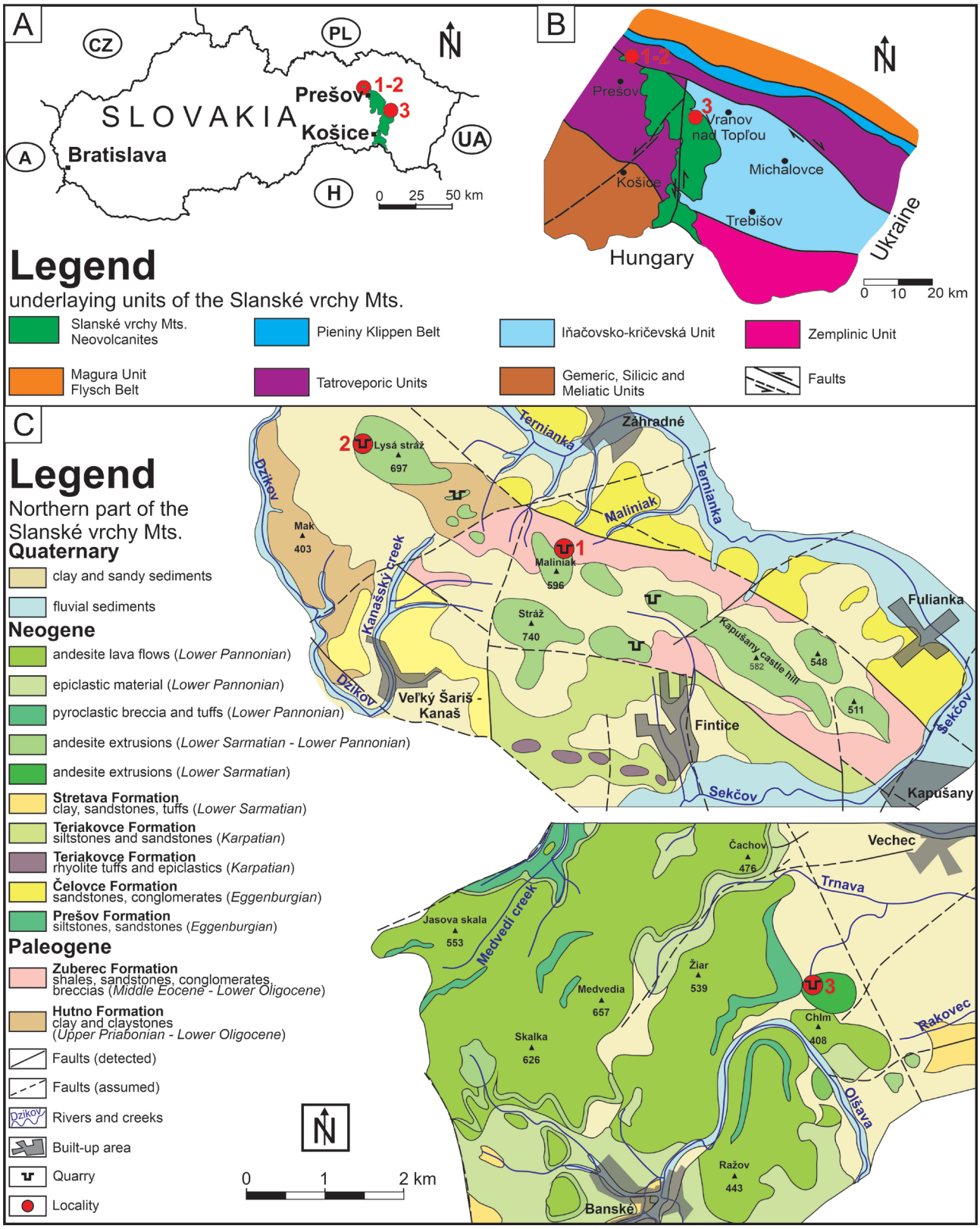

Fig. 1. A — Map of Slovakia with highlighted Slanské vrchy Mts. **B** — Geological map of the Eastern Slovakia with occurrence of underlying units (modified after Vass et al. 2000) under the Slanské vrchy Mts. neovolcanites. **C** — Details of the geological maps of the northern part of the Slanské vrchy Mts. (modified after Kaličiak et al. 1991) with the location of Hubošovce (1), Záhradné (2) and Vechec (3) quarries.

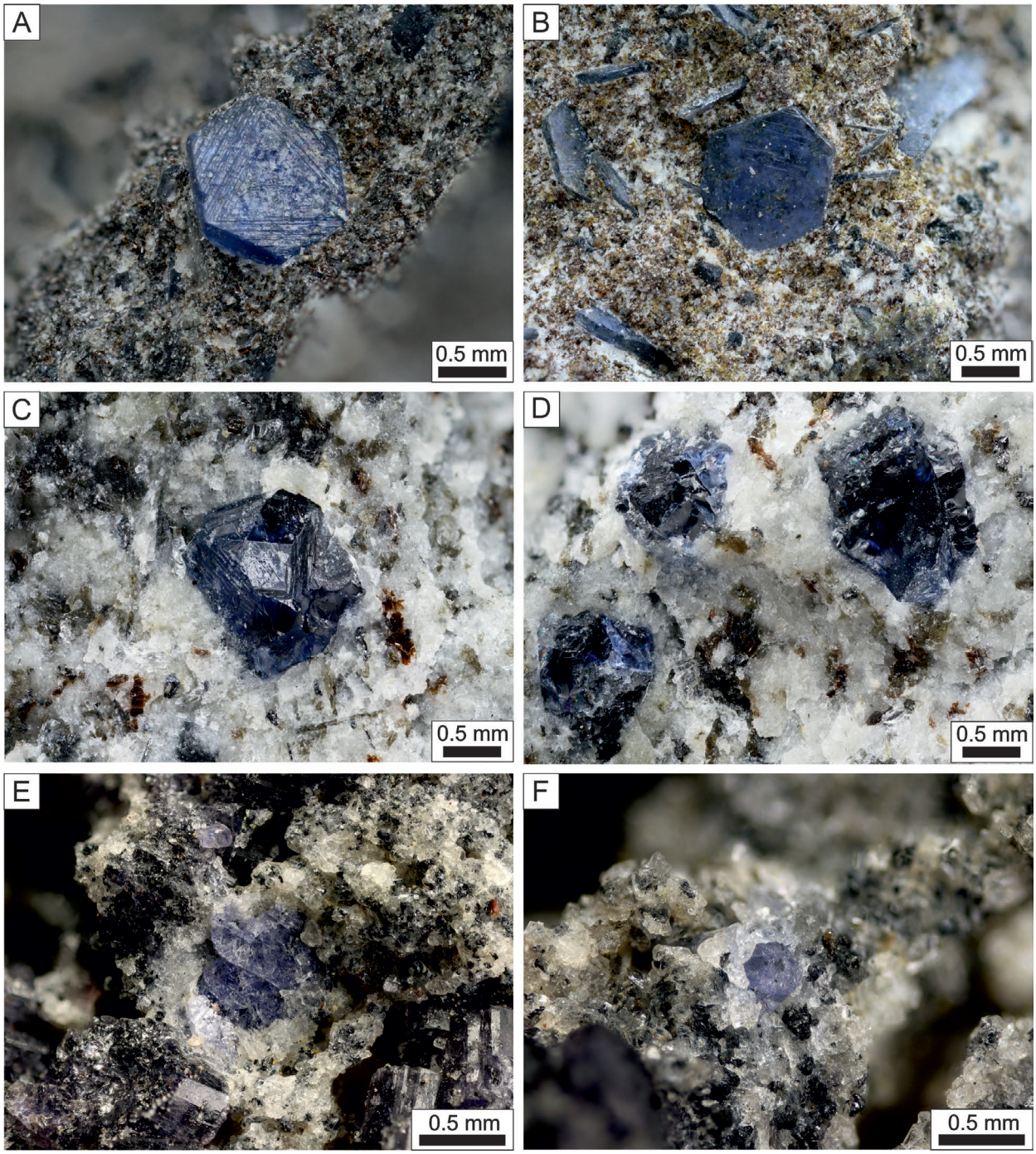

Fig. 2. Microphotographs of sapphires in xenoliths from studied localities. **A, B** — Pseudohexagonal tabular crystals of sapphire embedded in plagioclase–biotite matrix from Záhradné. **C, D** — Isolated complex crystals of sapphire embedded in plagioclase–biotite matrix from Hubošovce. **E, F** — Isolated tabular and pseudohexagonal crystals in plagioclase matrix with cordierite from Vechec. Photos by J. Demian (Záhradné, Hubošovce) and Ľ. Hrdlovič (Vechec).

coordinates are 49°04’17.5”N and 21°15’41.3”E. The Hubošovce quarry is founded at the edge of the Lysá Stráž extrusive body, located 3.5 km NE of Záhradné and 1.5 km SW of Hubošovce with GPS coordinates 49°05’08.8”N and 21°13’25.1”E. Vechec quarry is situated approximately 45 km SE of Prešov and 2.5 km SW of the Vechec village near the Vranov nad Topľou, with GPS coordinates estimated as 48°51’9.58”N, 21°36’12.10”E.

Xenolith samples from Záhradné and Hubošovce were collected in the period of years 2021 and 2022 by one of the authors (PM), which contained visible crystals of sapphires on the 1st and 2nd level of the Záhradné quarry from spherical

blocks of andesite and from fresh blast pile at the 3rd level of Hubošovce andesite quarry, within andesite block with dimensions approximately 30×20 cm. The samples of corundum from cordierite-bearing xenoliths at the Vechec quarry were collected by Pavel Černý in 1974.

Analytical methods

Quantitative chemical (WDS) analyses of minerals were obtained using an electron microanalyser JEOL-JXA850FE (Earth Science Institute, Slovak Academy of Sciences, Banská Bystrica). The following conditions, standards and X-ray lines were used: acceleration voltage 15 kV, beam current 20 nA, beam diameter between 1–10 μm, ZAF correction: albite (Na Kα, Al Kα), apatite (P Kα), baryte (Ba Lα), celestine (Sr Lα), Cr_2O_3 (Cr Kα), diopside (Si Kα, Ca Kα, Mg Kα), fluorite (F Kα), gahnite (Zn Kα), hematite (Fe Kα), Ni_2Si (Ni Kα), orthoclase (K Kα), rhodonite (Mn Kα), rutile (Ti Kα), $ScVO_4$ (V Kα), tugtupite (Cl Kα) and YPO_4 (Y Lα). Elements which were analysed quantitatively and are below the detection limit are not listed in the tables. Photographic documentation of relationships between minerals was carried out in the BSE mode. Abbreviations of minerals used in this study are according to Warr (2021).

The Raman spectra of corundum was collected in the range 100–1000 cm^{-1} using a DXR dispersive Raman Spectrometer (Thermo Scientific) mounted on a confocal Olympus microscope (Department of Mineralogy and Petrology, National Museum, Prague). The Raman signal was excited by an unpolarised green 532 nm solid state, diode-pumped laser, and detected by a CCD detector. The experimental parameters were: 100× objective, 25 μm pinhole spectrograph aperture, 10 mW laser power level for sapphires from Záhradné and Hubošovce and an unpolarised green 780 nm solid state, diode-pumped laser, 100× objective, 50 μm pinhole spectrograph aperture and 21 mW laser power level for sapphire from the Vechec.

Trace elements in sapphire were determined by LA-ICP-MS (Department of Chemistry, Faculty of Science, Masaryk University, Brno) using a laser ablation system LSX-213 G2+ (CeETAC Technologies) operating with a wavelength of 213 nm coupled to quadrupole ICP-MS spectrometer Agilent 7900 (Agilent Technologies, Japan). The tablet samples were placed in a two-volume ablation cell HelEx II, and ablated material was carried out by helium flow (0.6 and 0.3 l/min). A sample gas flow of Ar was admixed to the He carrier gas flow after the laser ablation cell. Therefore, the total gas flow was 1.9 l/min. Optimization of LA-ICP-MS conditions was performed with the glass reference material NIST SRM 610 with respect to maximum S/N ratio and minimum oxide formation (ThO^+/Th^+ counts ratio 0.2 %, U^+/Th^+ counts ratio 1.1 %). The LA-ICP-MS measurements used a single-hole drilling mode for 60 s for each spot. Laser ablation was performed with a laser spot diameter of 65 μm, laser fluency of 8 $J \cdot cm^{-2}$ and repetition rate of 10 Hz.

Results

Physical properties, chemical composition and spectroscopic characteristics of sapphires

Sapphires from all localities are dark blue to light blue with vitreous to diamond lustre and no visible pleochroic colour change. Sapphires from the ***Záhradné quarry*** occur in the form of tabular euhedral crystals up to 2.0 mm in size, which are composed of a pair of hexagonal faces developed parallel to each other and six faces perpendicular to the *Z* axis of hexagonal plates. These faces correspond to basal pinacoidal {0001} and hexagonal prismatic {1010} faces. Locally triangle-shaped lamellar patterns are visible along the c axis (Fig. 2a, b). Sapphire from the ***Hubošovce quarry*** xenoliths forms anhedral to subhedral crystals up to 1.5 mm in size, which show a more complexly developed habit consisting of two hexagonal faces grown parallel to each other, which correspond to basal pinacoidal {0001} faces connected with hexagonal dipyramids $\{hh\bar{2}hl\}$ and rhombohedral $\{10\bar{1}1\}$ faces (Fig. 2c) forming accumulations of isolated crystals (Fig. 2d). Corundum from the ***Vechec quarry*** cordierite-bearing xenoliths occurs in the form of tabular subhedral crystals up to 1 mm in size. The scarcity of macroscopically identified sapphires allows us to identify only basal pinacoidal {0001} faces (Fig. 2e) with triangular-shaped figures on crystal faces, one smaller crystal (up to 0.3 mm in size) rarely shows more complex crystal habits (Fig. 2f).

Quantitative chemical analyses show that the sapphires from the Záhradné quarry have a typical composition of 98.12–99.60 wt. % Al_2O_3 with increased contents of FeO (up to 0.40 wt. %) TiO_2 (up to 0.22 wt. %) and Cr_2O_3 (up to 0.07 wt. %). Sapphires from the Hubošovce quarry are composed of 98.45–99.39 wt. % Al_2O_3 with increased contents of FeO (up to 0.33 wt. %), TiO_2 (up to 0.41 wt. %) and Cr_2O_3 (up to 0.10 wt. %). Similarly, sapphires from the Vechec quarry reflect a stable chemical composition with 98.34–99.07 wt. % Al_2O_3 and increased FeO (up to 0.38 wt. %), TiO_2 (up to 0.29 wt. %) and Cr_2O_3 (up to 0.11 wt. %) contents. Other components examined by WDS analyses (V_2O_3, NiO and ZnO) are present only in minor concentrations (Table 1).

LA-ICP-MS analyses of sapphires confirm a higher average concentration of Fe (~2800 ppm) analysed in the range 2166–4687 ppm from Záhradné, slightly lower average concentration of Fe (average ~2500 ppm) identified in the range 1857–3051 ppm from Vechec and the lowest average concentration of Fe (~2300 ppm) in the range 1934–2666 ppm from Hubošovce. The highest concentration of Ti was observed in sapphires from Hubošovce (average ~2700 ppm) compared to those from Záhradné and Vechec (average ~1000 ppm Ti). All localities show increased contents of Cr (max ~750 ppm), V (max ~390 ppm) and Mg (max ~370 ppm). Ca, Na and K are present at ~100 ppm; higher concentration may be caused by plagioclase inclusions. The highest concentration of Ga was identified in samples from Hubošovce (up to 132 ppm); lower values in the range of 55–97 ppm were in Záhradné and

Table 1: Quantitative chemical microanalyses (in wt. %) of corundum from Záhradné, Hubošovce and Vechec.

Locality	Analysis	Al_2O_3	FeO	Cr_2O_3	V_2O_3	TiO_2	NiO	ZnO	Total
Záhradné	ZA-10_1	98.78	0.29	0.03	0.00	0.20	0.03	0.00	99.32
	ZA-10_2	99.11	0.15	0.04	0.00	0.13	0.00	0.00	99.44
	ZA-10_3	98.66	0.35	0.06	0.03	0.00	0.00	0.02	99.13
	ZA-10_4	98.12	0.34	0.04	0.00	0.22	0.00	0.00	98.72
	ZA-10_5	99.13	0.25	0.03	0.02	0.00	0.00	0.00	99.43
	ZA-10_6	99.11	0.24	0.06	0.00	0.13	0.02	0.00	99.55
	ZA-10_7	98.42	0.31	0.07	0.00	0.09	0.00	0.04	98.93
	ZA-10_8	99.11	0.25	0.06	0.00	0.04	0.00	0.00	99.46
	ZA-10_9	99.60	0.32	0.02	0.00	0.12	0.00	0.00	100.06
	ZA-10_10	99.08	0.40	0.07	0.00	0.17	0.00	0.00	99.72
Hubošovce	HU-1_1	99.08	0.18	0.10	0.00	0.05	0.00	0.00	99.41
	HU-1_2	99.09	0.24	0.05	0.02	0.28	0.02	0.00	99.70
	HU-1_3	99.39	0.24	0.05	0.00	0.32	0.00	0.00	99.99
	HU-1_4	99.27	0.33	0.02	0.00	0.22	0.00	0.02	99.86
	HU-1_5	99.20	0.25	0.05	0.02	0.12	0.00	0.00	99.64
	HU-1_6	99.08	0.32	0.03	0.03	0.37	0.03	0.00	99.86
	HU-1_7	98.70	0.31	0.00	0.00	0.19	0.00	0.02	99.21
	HU-1_8	99.02	0.21	0.00	0.00	0.41	0.00	0.03	99.67
	HU-1_9	98.91	0.27	0.00	0.00	0.22	0.00	0.00	99.39
	HU-1_10	98.45	0.33	0.02	0.00	0.28	0.00	0.00	99.09
Vechec	VEK-1_1	98.34	0.23	0.05	0.04	0.10	0.02	0.00	98.77
	VEK-1_2	98.59	0.25	0.09	0.05	0.09	0.01	0.06	99.14
	VEK-1_3	98.71	0.34	0.08	0.04	0.16	0.00	0.06	99.38
	VEK-1_4	98.82	0.26	0.05	0.06	0.00	0.01	0.00	99.20
	VEK-1_5	98.53	0.25	0.11	0.02	0.29	0.00	0.00	99.21
	VEK-1_6	98.71	0.26	0.08	0.02	0.11	0.00	0.00	99.17
	VEK-1_7	98.64	0.22	0.06	0.02	0.09	0.00	0.02	99.05
	VEK-1_8	98.65	0.19	0.10	0.01	0.04	0.03	0.00	99.02
	VEK-1_9	99.07	0.37	0.05	0.05	0.09	0.02	0.00	99.65
	VEK-1_10	99.00	0.38	0.08	0.02	0.00	0.02	0.00	99.49
	VEK-1_11	98.44	0.28	0.05	0.02	0.08	0.00	0.02	98.88
	VEK-1_12	98.84	0.32	0.05	0.03	0.12	0.00	0.03	99.39
	VEK-1_13	98.72	0.26	0.04	0.00	0.11	0.00	0.00	99.14

Vechec samples. Boron maintains stable values on average ~40 ppm. The average ΣREE is ~1.5 ppm, higher observed values (above 11.5 ppm) are possibly caused by inclusions of REE-rich minerals (Table 2). The concentrations of other elements are close (Mn, Zn, Ba, Ge, Li, Zr, As, Th, U) or bellow detection limit (Ni, Co, Pb, Cu, Rb, Sr, Nb, Cs and W) of LA-ICP-MS. Concentrations of Y+REE (La, Ce, Pr, Nd, Sm, Eu, Gd, Tb, Dy, Ho, Er, Tm, Yb, Lu, Hf and Ta) are shown in Supplementary Table S1.

The Raman spectra of corundum from all localities are given in Fig. 3a. The main bands observed are (in wavenumbers) 382, 385, 419, 450, 476, 648, 650, 706, and 710 cm^{-1}. The strongest band is at 419 cm^{-1}.

Mineralogy of the corundum-bearing xenoliths

Sapphire from Záhradné and Hubošovce occurs in micaceous metamorphic xenoliths, which are built mostly of biotite (annite–phlogopite series), quartz, K-feldspar and plagioclase. Minor orthopyroxene, hercynite, ilmenite, Ti-rich magnetite and accessory minerals such as fluorapatite, monazite-(Ce) and zircon were also observed. On the other hand, sapphire from Vechec occurs mainly in cordierite-bearing xenoliths associated with plagioclase, sillimanite and hercynite with ilmenite inclusions. Under BSE, all minerals except clinopyroxenes do not show chemical zoning and contain mineral inclusion such as monazite-(Ce) and zircon (Fig. 4a–f). The average chemical composition of studied minerals is shown in Table 3, and quantitative chemical analyses with corresponding formulae are shown in Supplementary Table S2a–g.

Corundum-bearing xenoliths from the ***Záhradné quarry*** dominantly contain biotite, K-feldspar, plagioclase and hercynite with corundum crystal embedded in plagioclase-rich parts. Biotite (Fig. 5a) is characteristic of the Mg (1.19–1.46 *apfu*) and Fe (1.08–1.43 *apfu*) content in approximately the same values at the *M* position. The atomic Mg/(Mg+Fe) is in the range 0.45–0.57 (Table 3, Suppl. Table S2), classifying micas as annite and phlogopite end-members. The *I* site is dominantly composed of K (0.83–0.91 *apfu*) with minor Na, Ca, Ba and vacancy. Ti content reaches maximum values of 0.28 *apfu* (Table 3, Suppl. Table S2). Two types of feldspars were identified (Fig. 5b), dominant presence of K-feldspar with average composition of $Or_{78}Ab_{21}An_1$ and plagioclase with dominant albite component and average composition of $Ab_{59}An_{40}Or_1$,

Table 2: LA-ICP-MS analyses of sapphire (in ppm) from the studied localities, Al_2O_3 and SiO_2 in wt. %, ΣREE*= Y+La+Ce+Pr+Nd+Sm+Eu+Gd+Tb+Dy+Ho+Er+Tm+Yb+Lu+Hf+Ta from Suppl. Table S1, symbol < means bellow detection limit.

Locality	Analysis	Al_2O_3	SiO_2	Ti	Cr	V	Fe	Mg	Mn	Zn	Ca	Na	K	Ba	Ga	Ge	B	Li	Zr	As	Th	U	ΣREE*
Záhradné	ZA10_1	98.45	1.00	1067	627	127	2983	128	1	2	<	28	35	1	71	2	67	<	1	3	0.1	0.3	3.4
	ZA10_3	98.65	0.89	1207	572	98	2358	109	<	1	<	28	31	0	55	2	30	6	0	3	0.1	1.6	4.5
	ZA10_5	98.57	0.92	1494	565	98	2425	114	<	1	32	38	37	0	62	2	40	3	0	2	0.0	0.1	6.2
	ZA10_6	98.50	1.03	1207	464	89	2417	80	<	1	<	41	46	0	64	<	23	<	0	2	0.0	0.5	0.9
	ZA10_7	98.48	1.12	784	204	97	2343	96	<	1	45	59	38	0	59	1	40	5	0	1	0.0	<	0.3
	ZA10_9	98.19	1.00	643	570	104	4687	313	37	5	19	1308	21	203	63	2	52	22	0	2	0.2	0.1	11.5
	ZA10_10	98.42	1.17	567	288	82	2166	97	63	<	71	105	48	0	55	2	43	7	0	2	0.1	1.7	144.8
Hubošovce	HU1_1	97.80	1.60	2344	404	163	2284	177	<	5	52	118	67	0	110	2	34	5	0	2	0.1	<	0.8
	HU1_2	97.71	1.77	1147	468	196	2666	146	<	4	60	145	83	0	132	2	50	4	<	2	<	0.0	0.9
	HU1_3	97.71	1.70	2439	442	180	2187	178	1	6	74	121	70	<	125	2	25	<	0	2	0.0	<	0.5
	HU1_4	97.95	1.60	1421	426	140	1977	128	<	4	49	130	70	<	104	<	27	6	0	3	<	<	0.3
	HU1_5	97.41	1.85	3821	155	188	2523	225	<	7	69	129	85	0	130	1	19	5	0	2	0.3	<	1.4
	HU1_6	97.54	1.80	3154	248	199	2177	198	<	5	73	136	86	<	117	2	42	5	0	3	0.1	<	0.5
	HU1_7	97.48	1.84	3172	240	167	2436	203	<	6	56	155	78	<	109	1	46	6	0	2	0.2	<	1.1
	HU1_8	97.42	1.85	3565	260	192	2451	225	<	7	68	174	92	<	115	<	42	7	1	2	0.4	<	1.7
	HU1_9	97.81	1.64	2549	228	171	1934	169	<	5	81	159	79	0	105	<	21	7	0	2	0.0	0.0	0.7
	HU1_10	97.44	1.85	3611	247	205	2219	234	<	5	53	180	94	<	112	<	24	7	0	2	0.1	<	0.7
Vechec	VEK1_A1	99.08	0.43	809	460	285	2364	260	4	20	38	66	45	0	97	2	72	6	0	5	0.1	0.0	0.3
	VEK1_A2	98.74	0.71	1317	455	227	2781	328	2	2	58	42	59	0	97	3	53	<	1	4	0.5	0.1	1.2
	VEK1_A4	98.97	0.57	850	357	193	2234	282	5	2	23	55	129	2	82	2	85	5	21	5	0.7	0.1	2.5
	VEK1_A7	98.65	0.91	503	776	389	1857	173	1	1	<	214	299	0	79	1	76	<	0	4	0.1	0.0	0.2
	VEK1_A13	96.28	2.91	1279	413	298	2258	210	8	2	590	1777	911	177	68	<	48	7	3	3	0.7	0.1	35.6
	VEK1_A14	97.18	2.07	1280	731	360	3061	234	28	6	84	664	678	8	90	<	108	<	16	7	1.0	0.3	2.7
	VEK1_1	99.47	<	1123	421	273	2575	372	2	3	72	94	38	0	93	3	6	<	0	4	0.0	<	1.2
	VEK1_3	99.45	<	1063	374	212	2496	252	<	1	40	30	15	<	63	2	10	<	0	2	0.0	<	1.0
	VEK1_4	99.48	<	991	630	219	2425	229	1	<	<	41	14	<	78	1	25	<	<	5	0.0	<	0.5
	VEK1_5	99.39	<	749	746	298	3051	228	3	1	88	38	34	2	71	<	18	<	1	8	0.0	<	3.0

locally enriched in Sr (up to 0.26 wt. % SrO; Table 4, Suppl. Table S2). In the xenolith matrix, hercynite anhedral, subhedral to euhedral crystals in size up to 0.3 mm were identified. Hercynite is composed dominantly by Fe^{2+} (up to 0.76 *apfu*) with minor Mg (up to 0.27 *apfu*), Mn and Zn in the A^{2+} position. The B^{3+} position is mostly occupied by Al (1.73–1.93 *apfu*) with minor content of Fe^{3+} (up to 0.25 *apfu*; Table 3, Suppl. Table S2). Hercynite crystals contain small (1–3 μm) inclusions of fluorapatite, monazite-(Ce) and zircon identified by EDS. Hercynite crystals are rarely overgrown by K-feldspar and biotite, often chloritized along the edges.

Corundum-bearing xenoliths from the ***Hubošovce quarry*** dominantly contain biotite, K-feldspar, plagioclase and hercynite with corundum crystals embedded in fine-grained biotite- and plagioclase-rich parts. Biotite (Fig. 5a) contains an increased content of Mg (1.69–1.87 *apfu*) and relatively stable content of Fe (0.98–1.14 *apfu*) in the *M* position. The atomic Mg/(Mg+Fe) is in the range 0.60–0.65 (Table 3, Suppl. Table S2) as phlogopite end-member prevails. The *I* site is dominantly composed of K (0.86–0.89 *apfu*) with minor Na, Ca, Ba and vacancy, whereas Ti content reaches maximum values of 0.19 *apfu* (Table 3, Suppl. Table S2). Three types of feldspars were identified (Fig. 5b), with the dominant presence of euhedral to anhedral plagioclase crystals, which occur in the xenolith matrix. They have variable chemical compositions corresponding to average formulae $Ab_{67}An_{28}Or_5$ and $An_{63}Ab_{36}Or_1$ for albite-dominant plagioclase and to $Or_{77}Ab_{21}An_1$ for K-feldspar (Table 4, Suppl. Table S2). Less abundant are subhedral porphyroblasts of zonal orthopyroxenes (up to 1 cm in size) in xenolith. Central parts are composed of enstatite ($En_{50–51}$) and continuously transit to ferrosilite ($Fs_{50–74}$) along the rim of the crystals. Wollastonite molecule is present in minimal values up to 2 mol. %. Corundum crystals from Hubošovce are overgrown by a thin, in BSE

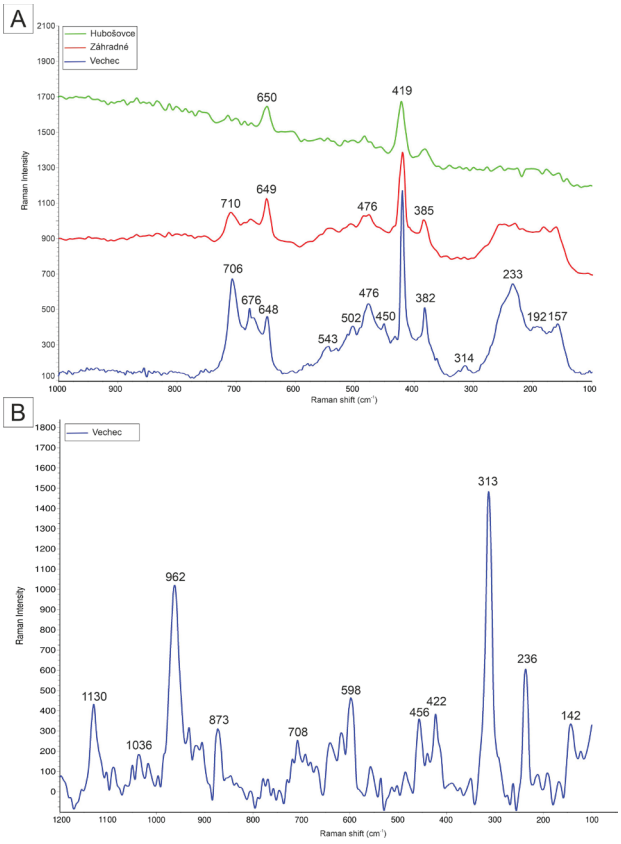

Fig. 3. Raman spectra of: **A** — Corundum from all studied localities in the range 100–1000 cm^{-1}. **B** — Sillimanite from the Vechec in the range 100–1200 cm^{-1}.

imaging light grey layer formed by hercynite. Chemically, hercynite is composed of Fe^{2+} (up to 0.73 *apfu*) with minor Mg (up to 0.27 *apfu*) in the A^{2+} position, whereas the B^{3+} position is mostly occupied by Al (up to 1.95 *apfu*) with very low content of Fe^{3+} (up to 0.07 *apfu*). Xenoliths are rich in 0.1 mm crystals of accessory ilmenite and Ti-rich magnetite with the content of Ti reaching up to 0.30 *apfu* and minor Mn and Mg content (up to 0.01 *apfu*; Table 3, Suppl. Table S2). In addition, small (1–3 μm) accessory grains of monazite-(Ce) and zircon were identified by EDS analysis.

Xenoliths with corundum from the ***Vechec quarry*** dominantly consist of cordierite, plagioclase and sillimanite with minor hercynite and ilmenite inclusions, where corundum is embedded mostly in plagioclase-rich parts. Cordierite macroscopically forms dark blue to purple barrel-shaped crystals (Fig. 2e). Cordierite is chemically homogeneous with dominant Mg content in the range 1.00–1.22 *apfu* and minor Fe content (0.80–1.00 *apfu*) with increased K (up to 0.15 *apfu*) and Na (up to 0.05 *apfu*, the atomic Mg/(Mg+Fe) is in the range 0.50–0.61 (Table 3, Suppl. Table S2). Plagioclase dominantly occurs with an average chemical composition corresponding to $Ab_{59}An_{26}Or_{14}$ (Table 4, Suppl. Table S2; Fig. 2b). Needle-like crystals of sillimanite with size up to 1 mm were observed as an abundant admixture in plagioclase and cordierite grains with a chemical composition close to ideal end-member formula, only slightly increased content of Fe (up to 0.04 *apfu*) was observed. The presence of sillimanite was confirmed by Raman spectroscopy (Fig. 3b). Accessory ilmenite is dominantly composed of ilmenite molecule (up to 93.70 mol. %) with minor geikielite (up to 5.46 mol. %) and pyrophanite (up to mol. 1.94 %) component and slightly higher content of V (up to 0.04 *apfu*). The composition of hercynite is characterised by dominant Fe^{2+} (up to 0.76 *apfu*) with minor Mg (up to 0.25 *apfu*) in the A^{2+} position. The B^{3+} position is mostly occupied by Al (up to 1.96 *apfu*) with very low content of Fe^{3+} (up to 0.04 *apfu*; Table 3, Suppl. Table S2). Abundant hercynite and ilmenite inclusions cause black colour of some xenolith parts (Fig. 2e, f).

Discussion and conclusions

Raman spectroscopy of sapphire

The blue colour of sapphires is caused by the presence of chromophore elements Fe and Ti in the crystal lattice (Simonet et al. 2008), supported by contents of these elements confirmed by EPMA-WDS (Table 1) and LA-ICP-MP analyses (Table 2). Raman spectroscopy of sapphire has been studied by multiple authors, who identified two A_{1g} and five E_g Raman active phonon modes at or close to 378, 418, 431, 450, 578, 645 and 750 cm^{-1} (e.g., Ashkin et al. 1968; Watson et al. 1981; Zouboulis et al. 1998). The strongest bands at 419 cm^{-1} A_{1g} mode and 384 cm^{-1} E_g mode are displacements caused by internal structural deformation (Zhao et al. 2021). These are characteristic bands of corundum. The shift of the A_{1g} mode at 650 cm^{-1} was also determined. Other E_g modes are assigned to the internal and external (rotations or translations) Al_2O_3 crystal vibrations (Porto & Krishnan 1967). Other minor bands identified by Raman analyses may be assigned to the mineral inclusions.

Genesis of sapphire and corundum-bearing xenoliths

The most widespread and generally established way of interpreting corundum genesis is based on the content of trace elements such as Fe, Ti, Cr, Ga and Mg and their ratios observed by LA-ICP-MS. These elements are used to discuss the magmatic versus metamorphic origin of sapphire in corundum-bearing xenoliths from studied localities Záhradné, Hubošovce and Vechec. Magmatic sapphire from alkali basalts shows increased content of Fe (2000–11000 ppm) and Ga (>140 ppm) with decreased contents of Cr (<40 ppm) and Mg (<20 ppm) compared to those of metamorphic origin with low Fe (<3000 ppm) and Ga (<75 ppm) contents and higher Mg (>60 ppm) content (Peucat et al. 2007). These geochemical characteristics reflect crystallization of sapphire in Mg-low and Ga-rich melts produced by aluminous alkaline magmas versus interaction of metamorphic aluminous layers with Mg-rich components via fluid circulation.

The studied sapphire from xenoliths at the Záhradné and Hubošovce localities occur in biotite and feldspathic lithology, whereas Vechec sapphire-bearing xenoliths are represented by cordierite with sillimanite, spinel and minor biotite assemblage. The content of trace elements in sapphire from all investigated occurrences is relatively similar, with increased content of Cr (~160–780 ppm), Ga (~60–130 ppm) and Mg (~80–330 ppm) indicating rather metamorphic origin.

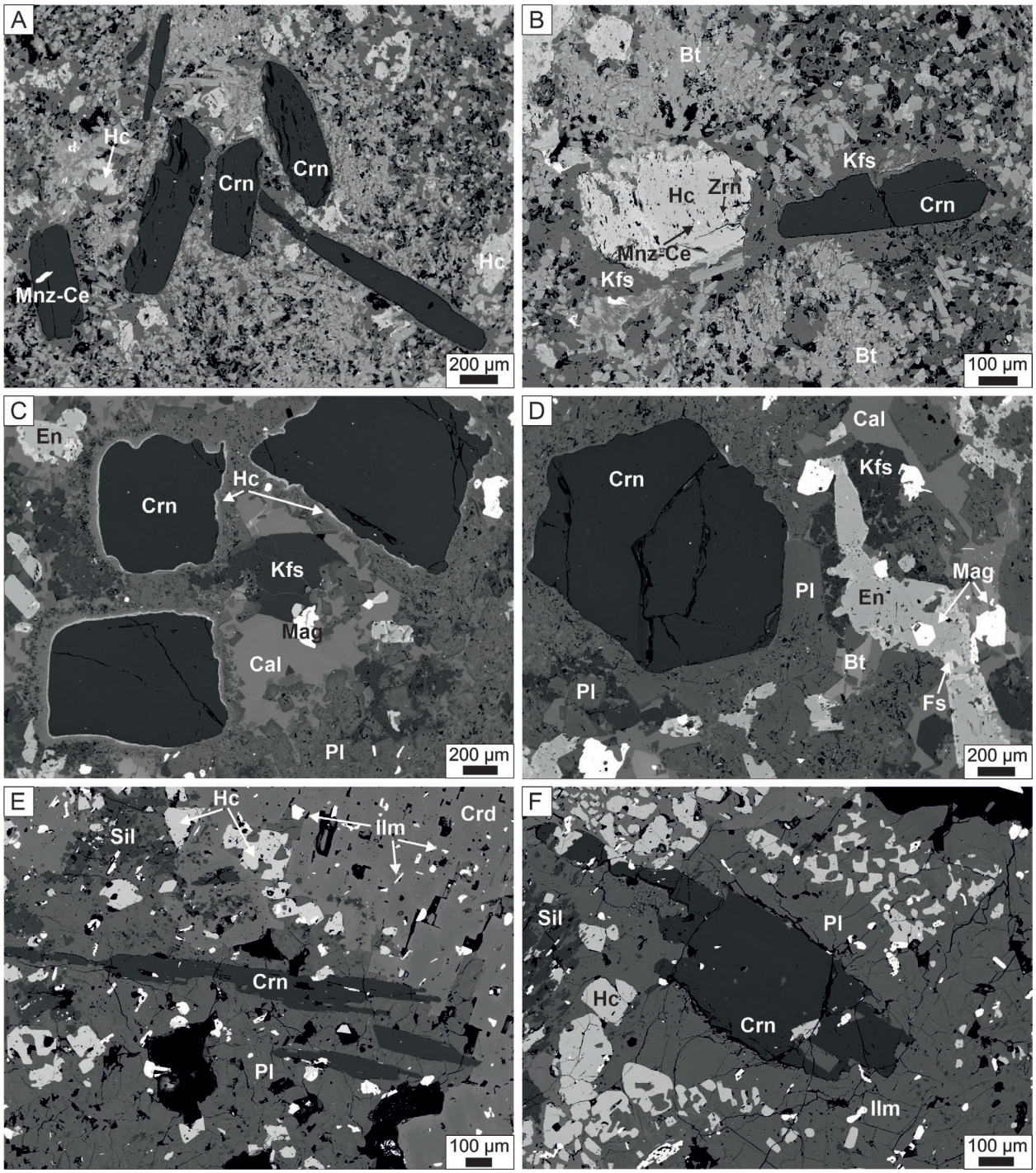

Fig. 4. BSE images of corundum-bearing xenolith from Záhradné (A, B), Hubošovce (C, D) and Vechec (E, F): **A** — Tabular corundum crystals in biotite-Kfs matrix with small inclusions of monazite-(Ce) and anhedral crystals of hercynite. **B** — Hercynite subhedral crystal with monazite-(Ce) and zircon inclusions in association with corundum in biotite-Kfs matrix. **C** — Corundum subhedral crystals overgrown by thin hercynite layer in xenolith matrix. **D** — Zonal enstatite-ferosilite crystal in biotite-plagioclase matrix in association with corundum. **E** — Tabular corundum crystals in plagioclase-cordierite matrix with abundant hercynite and ilmenite inclusions and fine sillimanite crystals. **F** — Corundum crystal in plagioclase matrix with abundant hercynite and ilmenite inclusions. Photo by T. Mikuš.

Table 3: Average chemical composition (in wt. %) and corresponding calculated empirical formulae of biotite, pyroxene, spinel, ilmenite, cordierite and sillimanite from corundum-bearing xenoliths from Záhradné, Hubošovce and Vechec.

Locality	Záhradné		Hubošovce						Vechec			
Mineral	Biotite	Hercynite	Biotite	Enstatite	Ferosilite	Magnetite	Ilmenite	Hercynite	Cordierite	Sillimanite	Hercynite	Ilmenite
Number of analyses	20	11	20	6	15	3	8	11	10	8	9	7
SiO_2	34.35	0.00	39.35	49.19	48.71	0.04	0.00	0.01	47.09	34.99	0.03	0.05
TiO_2	4.18	0.13	3.04	0.16	0.09	9.84	52.67	0.21	0.05	0.37	0.32	53.71
Al_2O_3	17.82	54.39	11.58	3.13	1.60	2.06	0.04	58.61	33.60	63.81	58.76	0.13
Cr_2O_3	0.04	0.15	0.06	0.11	0.08	0.58	0.13	0.16	0.00	0.03	0.08	0.13
V_2O_3	0.00	0.08	0.00	0.15	0.08	1.02	0.39	0.17	0.00	0.01	0.19	0.91
Fe_2O_3	–	7.39	–	0.00	0.00	44.99	–	2.55	–	–	1.48	–
FeO	19.53	30.54	16.80	28.21	34.13	39.26	48.07	30.53	10.17	0.58	32.00	45.08
MnO	0.16	0.52	0.13	0.48	0.91	0.33	0.72	0.19	0.28	0.01	0.41	0.88
MgO	11.86	5.93	16.16	16.63	12.84	0.09	0.38	6.39	7.21	0.05	5.61	1.31
NiO	–	0.04	–	0.05	0.02	0.05	0.01	0.08	0.01	0.00	0.12	0.03
ZnO	–	0.34	–	0.00	0.00	0.30	0.04	0.89	0.02	0.01	0.35	0.05
CaO	0.03	–	0.04	0.55	0.43	–	–	–	0.00	0.00	0.00	0.00
BaO	0.30	–	0.11	0.00	0.00	–	–	–	–	–	–	–
Na_2O	0.40	0.00	0.59	0.00	0.01	–	–	0.00	0.07	0.08	0.00	0.00
K_2O	9.32	–	9.32	0.00	0.00	–	–	–	0.28	0.02	0.00	0.00
H_2O*	396	–	2.85	–	–	–	–	–	–	–	–	–
F	0.00	–	2.30	–	–	–	–	–	–	–	–	–
Cl	0.22	–	0.42	–	–	–	–	–	–	–	–	–
−O=F	0.00	–	−0.97	–	–	–	–	–	–	–	–	–
−O=Cl	−0.05	–	−0.09	–	–	–	–	–	–	–	–	–
Total	102.104	99.50	101.68	98.66	98.90	98.55	102.46	99.78	98.79	99.97	99.36	102.29
Si^{4+}	2.568	0.000	2.911	1.914	1.952	0.001	0.000	0.000	4.887	0.950	0.001	0.001
Al^{3+}	1.570	0.003	1.010	0.143	0.075	0.283	0.972	0.004	0.004	0.008	0.007	0.986
Ti^{4+}	0.235	1.830	0.169	0.005	0.003	0.093	0.001	1.930	4.111	2.043	1.947	0.004
Cr^{3+}	0.002	0.003	0.003	0.003	0.003	0.017	0.003	0.004	0.000	0.001	0.002	0.003
V^{3+}	0.000	0.002	0.000	0.005	0.002	0.031	0.008	0.004	0.000	0.000	0.004	0.018
Fe^{3+}	–	0.159	–	0.012	0.011	1.294	–	0.054	–	–	0.031	–
Fe^{2+}	1.221	0.730	1.040	0.913	1.139	1.254	0.987	0.713	0.883	0.013	0.752	0.921
Mn^{2+}	0.010	0.013	0.008	0.016	0.031	0.011	0.015	0.004	0.025	0.000	0.010	0.018
Mg^{2+}	1.321	0.252	1.782	0.965	0.764	0.005	0.014	0.266	1.115	0.002	0.235	0.048
Ni^{2+}	–	0.001	–	0.002	0.001	0.002	0.000	0.002	0.001	0.000	0.003	0.001
Zn^{2+}	–	0.007	–	–	–	0.008	0.001	0.018	0.001	0.000	0.007	0.001
Ba^{2+}	0.009	–	0.003	0.000	0.000	–	–	–	–	–	–	–
Ca^{2+}	0.002	–	0.003	0.023	0.018	–	–	–	0.000	0.000	0.000	0.000
Na^{+}	0.058	0.000	0.085	0.000	0.001	–	–	0.000	0.015	0.004	0.000	0.000
K^{+}	0.889	–	0.880	0.000	0.000	–	–	–	0.038	0.001	0.000	0.000
F^{-}	0.000	–	0.539	–	–	–	–	–	–	–	–	–
Cl^{-}	0.028	–	0.052	–	–	–	–	–	–	–	–	–
OH^{-}	1.972	–	1.409	–	–	–	–	–	–	–	–	–
Cat. Sum	7.885	3.000	7.895	4.000	4.000	3.000	2.000	3.000	11.080	2.072	3.000	2.000

Chemical formula of biotite was calculated on the basis of 11 oxygen atoms (*apfu).* Symbol * represents calculation of H_2O from $(OH)^-$. Chemical formula of cordierite was calculated on the basis of 18 oxygen atoms (*apfu*) and sillimanite on the basis of 5 oxygen atoms (*apfu*). Chemical formulae of hercynite and Ti-magnetite were calculated on the basis of 3 cations, ilmenite on the basis 2 cations (*apfu*), pyroxene on the basis 4 cations (*apfu*).

The content of Fe is generally low (~1900–3000 ppm) with a locally slightly increased concentration (up to 4700 ppm) probably caused by hercynite, magnetite and/or ilmenite inclusions. Inclusions of other minerals are indicated by increased content of SiO_2 (up to 2.91 wt. %) and Na (~700, ~1300 and ~1800 ppm), Ca (~600 ppm), K (~900 and ~700 ppm) and Ba (~180 and ~200 ppm) in three analyses, however all sapphires show slightly increased Si (0.43–1.85 wt.%), Na (~30–210 ppm), Ca (~20–90 ppm) and K (~10–300 ppm) contents. REE-rich minerals are indicated by a dramatically increased content of REE in one analysis from the Záhradné, where ΣREE reaches ~145 ppm in contrast with a relatively small content of REE in other analyses (Table 2, Suppl. Table S2), possibly as the result of unidentified nano-inclusion(s) of REE-rich minerals (monazite, xenotime, etc.)

The metamorphic trend of sapphire from all corundum-bearing xenoliths is confirmed by classification diagrams defined by Sutherland et al. (2009) and Peucat et al. (2007). The Fe–Mg*100–Ti*10 triangular diagram (Fig. 6a) shows the nearly linear trend of sapphires out of the magmatic trend.

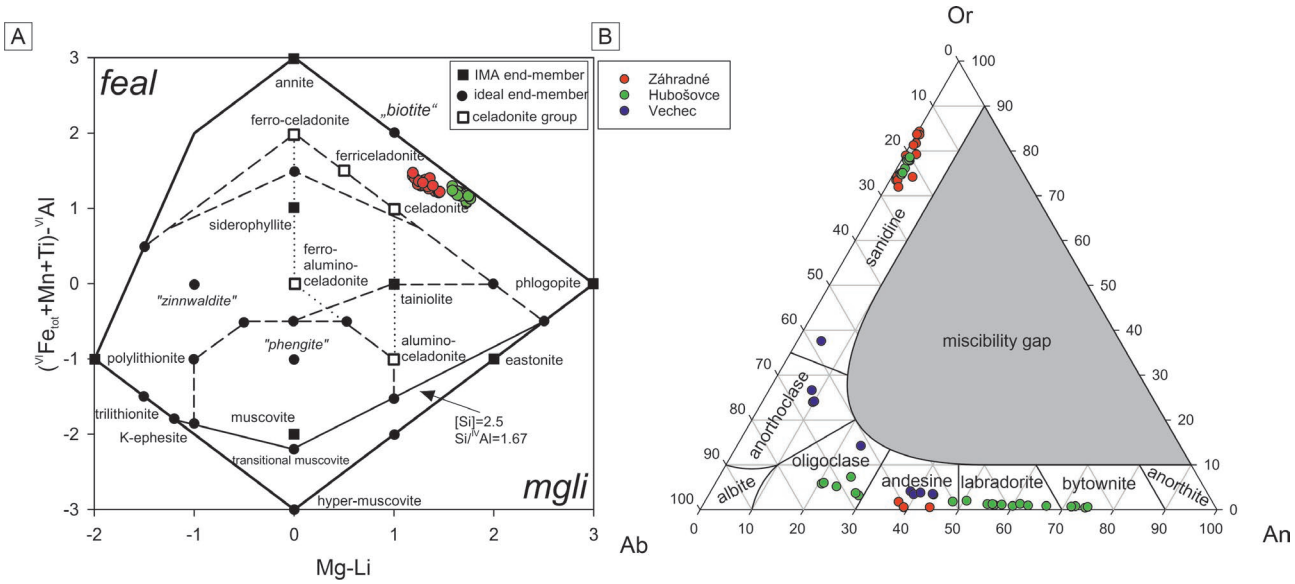

Fig. 5. Classification diagrams for micas (**A**) and feldspars (**B**) from the corundum-bearing xenoliths from Záhradné, Hubošovce and Vechec.

Table 4: Average chemical composition (in wt. %) and corresponding calculated empirical formulae of plagioclase and K-feldspars from corundum-bearing xenoliths from Záhradné, Hubošovce and Vechec.

Locality	**Záhradné**		**Hubošovce**			**Vechec**
Mineral	**Albite**	**Orthoclase**	**Albite**	**Anorthite**	**Orthoclase**	**Albite**
Number of analyses	4	16	7	14	9	10
P_2O_5	0.06	0.31	0.05	0.02	0.01	0.06
SiO_2	57.99	64.97	61.13	52.59	65.13	60.22
TiO_2	0.05	0.04	0.02	0.03	0.02	0.08
Al_2O_3	26.81	19.25	24.03	30.63	18.61	24.15
Fe_2O_3	0.30	0.34	0.16	0.15	0.09	0.16
MnO	0.01	0.02	0.02	0.02	0.01	0.02
MgO	0.02	0.00	0.01	0.01	0.00	0.01
BaO	0.01	0.12	0.11	0.00	0.24	0.38
SrO	0.23	0.06	0.08	0.08	0.07	0.13
CaO	8.28	0.26	5.99	12.79	0.29	5.30
Na_2O	6.77	2.39	7.93	4.13	2.41	6.66
K_2O	0.15	13.43	0.84	0.17	13.21	2.49
Total	100.67	101.20	100.37	100.63	100.07	99.65
P^{5+}	0.002	0.012	0.002	0.001	0.000	0.002
Si^{4+}	2.583	2.948	2.720	2.370	2.986	2.713
Ti^{4+}	0.002	0.001	0.001	0.001	0.001	0.003
Al^{3+}	1.407	1.029	1.260	1.627	1.005	1.283
Fe^{3+}	0.010	0.012	0.005	0.005	0.003	0.006
Sum *T*	4.004	4.001	3.987	4.004	3.995	4.007
Mn^{2+}	0.000	0.001	0.001	0.001	0.000	0.001
Mg^{2+}	0.001	0.000	0.001	0.001	0.000	0.000
Ba^{2+}	0.000	0.002	0.002	0.000	0.004	0.007
Sr^{2+}	0.006	0.002	0.002	0.002	0.002	0.003
Ca^{2+}	0.395	0.013	0.286	0.618	0.014	0.256
Na^{+}	0.585	0.211	0.684	0.361	0.214	0.582
K^{+}	0.008	0.777	0.048	0.010	0.773	0.143
Sum *M*	0.996	1.005	1.023	0.993	1.007	0.992
$NaAlSi_3O_8$ (Ab)	59	21	67	36	21	59
$CaAl_2Si_2O_8$ (An)	40	1	28	63	1	26
$KAlSi_3O_8$ (Or)	1	78	5	1	77	14

Chemical formulae of plagioclase and K-feldspars were calculated on the basis of 8 O atoms (*apfu*)

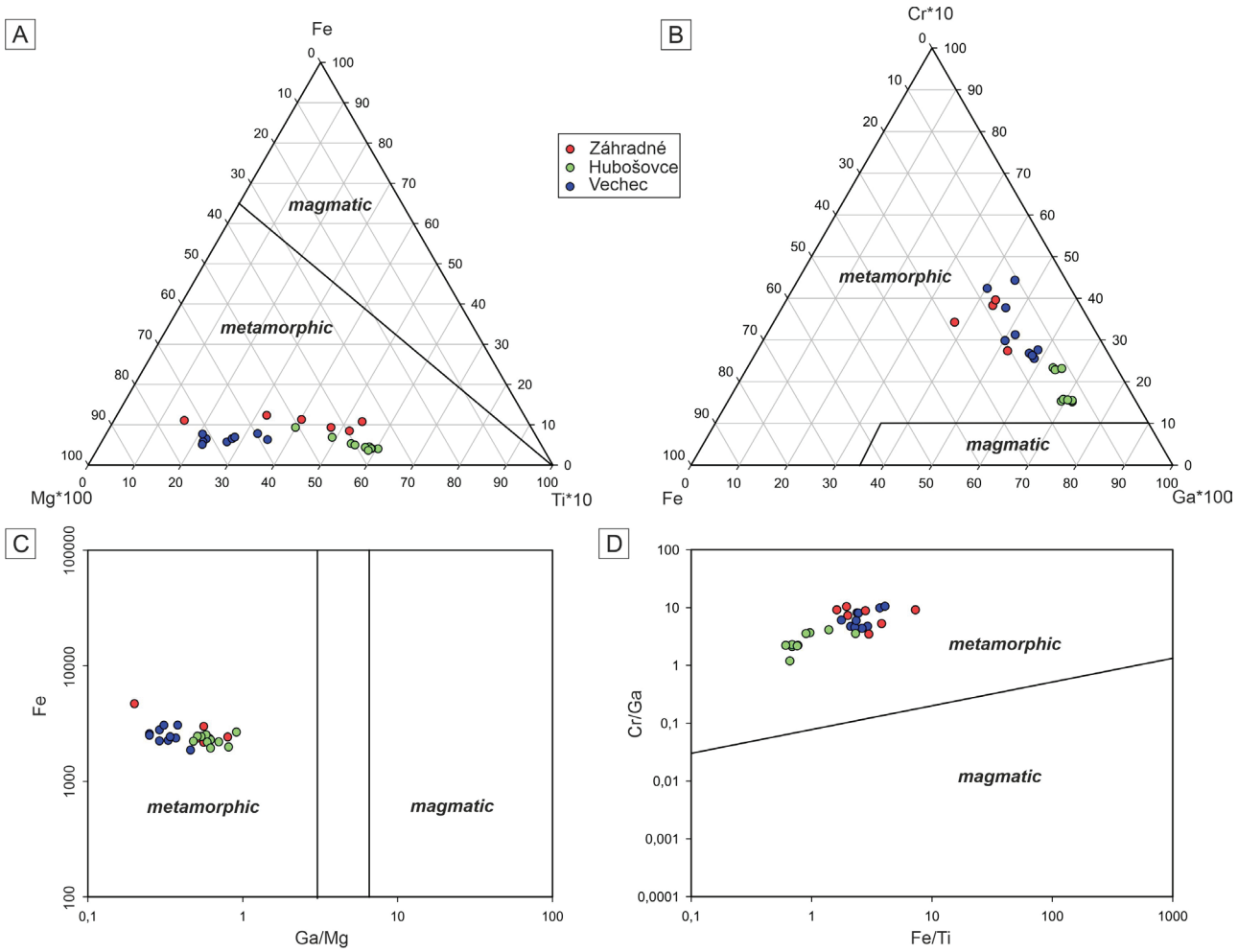

Fig. 6. Discrimination diagrams for metamorphic versus magmatic origin of corundum from Záhradné, Hubošovce and Vechec. All values are in ppm. **A** — Fe–Mg*100–Ti*10; **B** — Cr*10–Fe–Ga*100; **C** — Ga/Mg vs. Fe; **D** — Fe/Ti vs. Cr/Ga (modified after Sutherland et al. 2009 and Peucat et al. 2007).

The similar linear trend may be observed in the Cr*10–Fe–Ga*100 triangular diagram (Fig. 6b) where all sapphire samples fall to the discrimination field of metamorphic origin although with a closer trend towards magmatic origin compared to Fig. 6a. The same trend may be observed in binary diagrams created based on element concentrations and ratios, where the Ga/Mg versus Fe diagram (Fig. 6c) and the Fe/Ti versus Cr/Ga diagram (Fig. 6d) show the metamorphic origin of all studied corundum samples.

The formation of sapphire is caused by the existence of precursor aluminous minerals in Al-enriched zones of metasediments depleted in silica (Giuliani et al. 2014). Incorporation of these precursor sedimentary rocks into the magmatic reservoir caused their thermal overprint, indicated by significant increase of Ti (~ 0.2 *apfu*) in biotite as suggested by Henry et al. (2005); Ti content in biotite achieves 0.19–0.28 *apfu* Ti in Záhradné and slightly lower content in Hubošovce (0.14–0.19 *apfu* Ti; Table 3, Suppl. Table S2). Experimental synthesis of metapelites (Icenhower & London 1995) at the 200 MPa and H_2O-saturated system proved biotite stability in temperature interval 600–750 °C, with its progressive reaction to hercynite at the upper limits of the temperature range. These experiments showed corundum and orthoclase-rich feldspar originated from muscovite precursor representing primarily metamorphosed pelitic component at 650 °C with strong incorporation of Fe and Ti into the corundum crystals at above 700 °C. Increased content of boron (~10–110 ppm) and lithium (up to ~20 ppm) determined by LA-ICP-MS (Table 2) in sapphires supports this genetic assumption, and it is interpreted as a residual component embedded from possible mica precursor. Recently, white micas have been considered to be an important source of boron in subducted metasedimentary rocks (Guo et al. 2022).

Formation of ilmenite and Ti-rich magnetite in studied xenoliths resulted from high-temperature oxidation associated with melting and dehydration of micas (e.g., Grapes 1986; Johnson & Plank 1999; Sola et al. 2017). Furthermore, in association with sillimanite, amphibolite- to medium-pressure

granulite facies with metamorphic conditions corresponding to >300 MPa and 500–800 °C are important to meet the thermobaric conditions required for corundum crystallization (Simonet et al. 2008; Johnson et al. 2011). Increased content of anorthite molecule in plagioclase (Table 3, Suppl. Table S2) represents residuals after partial fractional melting of feldspars in precursor rocks caused by preferential dissolution of $NaAlSi_3O_8$ component in the initial plagioclase melts (Grapes 1986; Li et al. 2020). Partial melting of metapelitic xenoliths caused by biotite dehydration and concurrent melting causes simultaneous growth of cordierite, orthopyroxenes and spinel (Braun & Kriegsman 2001).

Sapphire crystals from the Hubošovce exhibit spinel coronal textures (Fig. 4c), which are typically developed from the destabilization of corundum during the retrograde development, as observed at Ambatomena ruby metamorphic occurrence in Madagascar (Giuliani et al. 2014).

It is considered that biotite-rich xenoliths from the Slanské vrchy Mts. Originated from the Čierna hora crystalline complex underlying Tertiary volcanic and sedimentary cover rocks (Košuth 2005). The formation of cordierite-rich xenoliths probably originated from the assimilation of Al-rich argillaceous rocks, which obliterates the metamorphic impact of crust metapelites (Košuth 2006) and by subsequent crystallization of Al–Fe–Mg(Ti)-enriched melt in the inner aureole of the magma chamber (Marcinčáková & Košuth 2011). Presence of sillimanite and corundum crystals in cordierite-rich xenoliths show preserved characteristic trace elements composition and paragenesis of metamorphic origin.

Comparison with corundum-bearing localities in the Western Carpathian region

The studied sapphires in corundum-bearing xenoliths from the Záhradné, Hubošovce and Vechec show metamorphic trend based on their geochemical data and minerals association. For comparison, different geochemical and genetic trends were detected in sapphires from the Cerová vrchovina Mts. Sapphires from Gortva and mostly from Hajnáčka were generated during the solidification from fractionated melt in the upper mantle or lower crust and subsequently transported to the surface in the form of syenite/anorthoclasite xenoliths (Uher et al. 2012). A closer genetic scenario compared to our localities is assumed for pink sapphires from Hajnáčka, where their composition suggests metamorphic origin, developed possibly from Paleozoic gneisses and migmatites of the Veporic Superunit (Uher et al. 2012). Corundum exsolutions were identified in xenoliths from the Cerová vrchovina Mts., which are interpreted as products of pyrometamorphic overprint from plagioclase by surrounding basalts (Reato et al. 2022). Similarly, thermally overprinted sedimentary xenoliths rich in plagioclase, biotite, sillimanite and acicular crystals of corundum from boreholes in the Javorie volcanic zone were interpreted as products of contact metamorphosis of pelitic sediments and diorite magma (Kollárová & Hraško 2009).

Acknowledgement: The authors are thankful to handling editor P. Bačík as well as reviewers P. Uher and P. Gadas for their suggestions, which helped us to improve manuscript. We are also thankful to J. Sejkora and L. Vrtiška who provided us with Raman spectra, and J. Demian and Ľ. Hrdlovič who provided us microphotographs of sapphires. We are also thankful to VSK MINERAL s.r.o., who allowed us to collect samples from the studied quarries and P. Černý who provided us with samples from Vechec. This work was supported by the VEGA Grant No. 2/0029/23.

References

Ashkin M., Parker J.H. & Feldman D.W. 1968: Temperature dependence of the Raman lines of α-Al_2O_3. *Solid State Communications* 6, 343–346. https://doi.org/10.1016/0038-1098(68)90152-X

Bacsó Z. 1971: New minerals and new raw material possibilities of Vihorlat. *Mineralia Slovaca* 3, 247–250 (in Slovak).

Bónová K. 2005: Mineralogy, petrology and P-T conditions of crystallization of the andesite body Maliniak and Lysá stráž of the Lysá stráž – Oblík Formation, eastern Slovakia. *Mineralia Slovaca* 37, 503–512 (in Slovak).

Böhmer M. & Šímová M. 1976: Contact-metasomatic aureole of Miocene intrusives in the Kremnica Mountains. *Acta Geologica et Geographica Universitatis Comenianae Geologica* 30, 119–137 (in Slovak).

Braun I & Kriegsman L.M. 2001: Partial melting in crustal xenoliths and anatectic migmatites: a comparision. *Physics and Chemistry of the Earth, Part A: Solid Earth and Geodesy* 26, 261–266. https://doi.org/10.1016/S1464-1895(01)00054-0

Derco J., Kozáč J. & Očenáš D. 1977: New data about minerals and genesis of secondary quartzites of the Kapka locality in central Vihorlat. *Mineralia Slovaca* 9, 185–205 (in Slovak).

Ďuďa R., Černý P., Kaličiak M., Kaličiaková E., Tözsér J., Ulrych J. & Veselovský F. 1981: Mineralogy of northern part of the Slanské Mountains. *Mineralia Slovaca – Monograph* 2, Bratislava, 1–99 (in Slovak).

Ďurica D., Kaličiak M., Kreuzer H., Müller P., Orlický O., Slávik J., Tözsér J. & Vass D. 1978: Sequence of volcanic events in Eastern Slovakia in the light of recent radiometric age determinations. *Bulletin of the Central Institute of Geology* 53, 75–88.

Fiala F. 1954: Some xenoliths of andesites from the Slovak Midmountains. *Sborník Ústředního Ústavu Geologického Oddelení, Geologie* 21, 309–357 (in Czech).

Giuliani G., Fallick A.E., Garnier V., France-Lanord C., Ohnenstetter D. & Schwarz D. 2005: Oxygen isotope composition as a tracer for the origins of rubies and sapphires. *Geology* 33, 249–252. https://doi.org/10.1130/G21261.1

Giuliani G., Ohnenstetter D., Fallick A.E., Groat L. & Fagan A.J. 2014: Chapter 2: The geology and genesis of gem corundum deposits. *Mineralogical Association of Canada Short Course* 44, 29–112.

Giuliani G., Groat L.A., Fallick A.E., Pignatelli I. & Pardieu V. 2020: Ruby Deposits: A Review and Geological Classification. *Minerals* 10, 597. https://doi.org/10.3390/min10070597

Grapes R.H. 1986: Melting and Thermal Reconstruction of Pelitic Xenoliths, Wehr Volcano, East Eifel, West Germany. *Journal of Petrology* 27, 343–396. https://doi.org/10.1093/petrology/27.2.343

Guo S., Su B., John T., Thao K., Tang P., Chen Y. & Li Y. 2022: Boron release and transfer inducted by phengite breakdown in subducted impure metacarbonates. *Lithos* 408–409, 106548. https://doi.org/10.1016/j.lithos.2021.106548

Henry D.J., Guidotti C.V. & Thompson J.A. 2005: The Ti-saturation surface for low-to-medium pressure metapelitic biotites: Implications for geothermomtry and Ti substitution mechanisms. *American Mineralogist* 90, 316–328. https://doi.org/10.2138/am.2005.1498

Hurai V., Simon K., Wiechert U., Hoefs J., Konečný P., Huraiová M., Pironon J. & Lipka J. 1998: Immiscible separation of metalliferous Fe/Ti-oxide melts from fractionating alkali basalt: PT-fO2 conditions and two-liquid elemental partitioning. *Contributions to Mineralogy and Petrology* 133, 12–29.

Huraiová M. & Konečný P. 2006: U–Pb–Th dating and chemical composition of monazite in xenoliths of syenite and pincinite from the Upper Miocene maar near the village of Pinciná (Lučenecká basin). *Mineralia Slovaca* 38, 141–150 (in Slovak).

Hvožďara P. & Činčár J. 1972: Corundum: an accessory mineral in the Central Slovak neovolcanics. *Zborník Pedagogický Fakulty Univerzity Šafárikovi, Přírodní Vědy* 11, 143–157 (in Slovak).

Icenhower J. & London D. 1995: An experimental study of element partitioning among biotite, muscovite, and coexisting peraluminous silicic melt at 200 MPa (H_2O). *American Mineralogist* 80, 1229–1251. https://doi.org/10.2138/am-1995-11-1213

Ishizawa N., Miyata T., Minato I., Marumo F & Iwai S. 1980: A structural Investigation of α-Al_2O_3 at 2170 K. *Acta Crystallographica Section B* 36, 228–230. https://doi.org/10.1107/S0567740880002981

Johnson M.C. & Plank T. 1999: Dehydration and melting experiments constrain the faith of subducted sediments. *Geochemistry, Geophysics, Geosystems* 1, 1007. https://doi.org/10.1029/1999GC000014

Johnson T.E., White R.W. & Brown M. 2011: A year in the life of an aluminous metapelite xenolith – The role of heating rates, reaction overstep, H_2O retention and melt loss. *Lithos* 124, 132–143. https://doi.org/10.1016/j.lithos.2010.08.009

Kaličiak M. & Repčok I 1987: Reconstruction of the time evolution of the volcanoes of the northern part of the Slanské vrchy Mts. *Mineralia Slovaca* 19, 401–415 (in Slovak).

Kaličiak M., Baňacký V., Jacko S., Janočko J., Karoli S., Molnár J., Petro Ľ., Priechodská Z., Syčev V., Škvarka L., Vozár J., Zlinská A & Žec B. 1991: Explanations fot the geological map of the Slanské vrchy Mts. and Košice basin – northern part, 1:50 000, *GÚDŠ*, Bratislava 1–239 (in Slovak).

Kollárová V. & Hraško Ľ. 2009: Mineralogy and petrology of the basement xenoliths in the boreholes from the Central Volcanic Zone of the Javorie Mts. *Mineralia Slovaca* 41, 457–476 (in Slovak).

Košuth M. 2005: Characterization of biotite xenoliths from Brestov, Slanské vrchy Mts. *Mineralia Slovaca*, 37, 367–369 (in Slovak).

Košuth M. 2006: New type of cordierite assemblages from the Slanské vrchy Mts., Eastern Slovakia. *Acta Mineralogica-Petrographica, Abstract Series* 5, 59.

Li Y., Yang Y., Liu Y-C., Groppo Ch. & Rolfo F. 2020: Muscovite Dehydration Melting in Silica-Undersaturated Systems: A Case Study from Corundum-Bearing Anatectic Rocks in the Dabie Orogen. *Minerals* 10, 213. https://doi.org/10.3390/min10030213

Marcinčáková Z. & Košuth M. 2011: Characteristics of Xenoliths in the East Slovakian Neogene Volcanites. *Analele Stiintifice ale Universitatii „Al. I. Cuza" din Iasi, Seria Geologie* 57, 17–27.

Marková M. & Štohl J. 1978: Some results about the solfatara formation in the Kalinka – Vígľašská Huta area. *Západné Karpaty, séria Mineralógia Petrografia Geochémia Metalogenéza* 5, 109–144 (in Slovak).

Miranda-Diáz G., Riveros-Jensen K., Heide G., Menzies A., Griem W., Araya-Tabilo E., Añasco-Leyton G. & Medina E. 2022: Geology and mineralogy of sapphire-rich metasomatites (sapphirites) deposit at the Portezuelo de Pajas Blancas, northern Chile: Genetic implications for unusual metasomatic processes in the Central Andes. *Ore Geology Reviews* 141, 104646. https://doi.org/10.1016/j.oregeorev.2021.104646

Pekov I.V., Anikin L.P., Chukanov N.V., Belakovskiy D.I., Yapaskurt V.O., Sidorov E.G., Britvin S.N. & Zubkova N.V. 2019: Deltalumite, a new natural modification of alumina with spinel-tpye structure. *Zapiski RMO (Proceedings of the Russian Mineralogical Society*) 148, 45–58. https://doi.org/10.30695/zrmo/2019.1485.02

Peucat J.J., Ruffault P., Fritsch E., Bouhnik-Le Coz M., Simonet C. & Lasnier B. 2007: Ga/Mg ratio as a new geochemical tool to differentiate magmatic from metamorphic blue sapphires. *Lithos* 98, 261–274. https://doi.org/10.1016/j.lithos.2007.05.001

Porto S.P.S. & Krishnan R.S. 1967: Raman Effect of Corundum. *The Journal of Chemical Physics* 47, 1009–1012. https://doi.org/10.1063/1.1711980

Reato L., Huraiová M., Konečný P., Marko F. & Hurai V. 2022: Formation of Esseneite and Kushiroite in Tschermakite-Bearing Calc-Silicate Xenoliths Ejected in Alkali Basalt. *Minerals* 12, 156. https://doi.org/10.3390/min12020156

Simonet C., Fritsch E. & Lasnier B. 2008: A classification of gem corundum deposits aimed towards gem exploration. Ore Geology Reviews 34, 127–133. https://doi.org/10.1016/j.oregeorev.2007.09.002

Singh B. & Gilkes R.J. 1995: The natural occurrence of χ-alumina in lateritic pisolites. *Clay Minerals* 30, 39–44. https://doi.org/10.1180/claymin.1995.030.1.04

Sola A.M., Hasalová P., Weinberg R.F., Suzano N.O., Becchio R.A., Hongn F.D. & Botelho N. 2017: Low-P melting of metapelitic rocks and the role of H_2O: Insights from phase equilibria modelling. *Journal of Metamorphic Geology* 35, 1131–1159. https://doi.org/10.1111/jmg.12279

Sorokina E.S., Karampelas S., Nishanbaev T.P, Nikadrov S.N. & Semiannikov B.S. 2017: Sapphire megacrysts in syenite pegmatites from the Ilmen Mountains, South Urals, Russia: New mineralogical data. *Canadian Mineralogist* 55, 823–843. https://doi.org/10.3749/canmin.1700016

Sutherland F.L., Zaw K., Meffre S., Giuliani G., Fallick A.E., Graham I.T. & Webb G.B. 2009: Gem-corundum megacrysts from east Australian basalt fields: trace elements, oxygen isotopes and origins. *Australian Journal of Earth Sciences* 56, 1003–1022. https://doi.org/10.1080/08120090903112109

Szakáll S., Udubaşa G., Ďuďa R., Kvasnytsya V., Koszowska E. & Novák M. 2002: Minerals of the Carpathians. *Granit*, Prague 1–480.

Tilley D.B. & Eggleton R.A. 1996: The natural occurrence of eta-alumina (η-Al2O3) in bauxite. *Clays and Clay Minerals* 44, 658–664. https://doi.org/10.1346/CCMN.1996.0440508

Uher P., Giuliani G., Szakáll S., Fallick A., Strunga V., Vaculovič T., Ozdín D. & Gregáňová M. 2012: Sapphires related to alkali basalts from the Cerová Highlands, Western Carpathians (southern Slovakia): composition and origin. *Geologica Carpathica* 63, 71–82. https://doi.org/10.2478/v10096-012-0005-7

Vass D., Elečko M., Janočko J., Karoli S., Pereszlenyi M., Slávik J. & Kaličiak M. 2000: Paleogeography of the East-Slovakian Basin. *Slovak Geological Magazine* 6, 377–407.

Warr L.N. 2021: IMA-CNMNC approved mineral symbols. *Mineralogical Magazine* 85, 291–320. https://doi.org/10.1180/mgm.2021.43

Watson G.H., Daniels W.B. & Wang C.S. 1981: Measurements of Raman Intensities and Pressure-Dependence of Phonom Frequencies in Sapphire. *Journal of Applied Physics* 52, 956–958. https://doi.org/10.1063/1.328785

Zhao Q-y., Xu Ch. & Liu X-y. 2021: Spectral Characteristics of Dark-Blue Corundum From Fangsan Mine, Shandong, China and Le-Shuza_Kone Mine, Mogok, Burma. *Spectroscopy and Spectral Analysis* 41, 629–635. https://doi.org/10.3964/j.issn.1000-0593(2021)02-0629-07

Zigert K., Shirokov A.L., Nikishova L.V., Pavlova L.A. & Babiy O.A. 1990: Natural analogues of the alumina modifications (δ-Al_2O_3 and θ-Al_2O_3) in permafrost-area sediments. *Transactions (Doklady) of the USSR Academy of Sciences. Earth Science Sections* 4, 221–225 (in Russian).

Zorkovský V. 1953: Petrographic-chemical nature of a garnet andesite from Záhradné (Sedikart) in the eastern Slovakia. *Geologica Carpathica* 3, 27–39 (in Slovak).

Zouboulis E., Renusch D. & Grimsditch M. 1998: Advantages of ultraviolet Raman scattering for high temperature investigations. *Applied Physics Letters* 72, 1–3. https://doi.org/10.1063/1.121437

Electronic supplementary material is available online:

Supplementary Table S1 at http://geologicacarpathica.com/data/files/supplements/GC-75-2-Myslan_TableS1.xlsx
Supplementary Table S2 at http://geologicacarpathica.com/data/files/supplements/GC-75-2-Myslan_TableS2.xlsx